

THE SANTA FE LIGHT CONE SIMULATION PROJECT: II. THE PROSPECTS FOR DIRECT DETECTION OF THE WHIM WITH SZE SURVEYS

ERIC J. HALLMAN^{1,2}, BRIAN W. O'SHEA³, BRITTON D. SMITH², JACK O. BURNS² & MICHAEL L. NORMAN⁴
Draft version November 3, 2018

ABSTRACT

Detection of the Warm-Hot Intergalactic Medium (WHIM) using Sunyaev-Zeldovich effect (SZE) surveys is an intriguing possibility, and one that may allow observers to quantify the amount of “missing baryons” in the WHIM phase. We estimate the necessary sensitivity for detecting low density WHIM gas with the South Pole Telescope (SPT) and Planck Surveyor for a synthetic 100 square degree sky survey. This survey is generated from a very large, high dynamic range adaptive mesh refinement cosmological simulation performed with the Enzo code. We find that for a modest increase in the SPT survey sensitivity (a factor of 2-4), the WHIM gas makes a detectable contribution to the integrated sky signal. For a Planck-like satellite, similar detections are possible with a more significant increase in sensitivity (a factor of 8-10). We point out that for the WHIM gas, the kinematic SZE signal can sometimes dominate the thermal SZE where the thermal SZE decrement is maximal (150 GHz), and that using the combination of the two increases the chance of WHIM detection using SZE surveys. However, we find no evidence of unique features in the thermal SZE angular power spectrum that may aid in its detection. Interestingly, there are differences in the power spectrum of the kinematic SZE, which may not allow us to detect the WHIM directly, but could be an important contaminant in cosmological analyses of the kSZE-derived velocity field. Corrections derived from numerical simulations may be necessary to account for this contamination.

Subject headings: cosmology: theory—galaxies:clusters:general—cosmology:observations—hydrodynamics—methods:numerical—cosmology:cosmic microwave background

1. INTRODUCTION

A significant fraction of baryons in the universe are expected to be in the Warm-Hot Intergalactic Medium (WHIM). Numerical cosmological simulations (e.g., Davé et al. 2001; Cen & Ostriker 1999) predict that somewhere around 30-40% of all baryons exist in this phase, characterized by electron temperatures between 10^5 and 10^7 K. This shock-heated gas primarily is located in large-scale filaments and sheets in the cosmic web, strung between clusters of galaxies. Observations of this gas (if collisional ionization is the correct interpretation) have been made in Ly α and OVI absorption (Tripp et al. 2008; Danforth & Shull 2005, 2008), and also are likely detectable in UV absorption lines and X-ray lines of OVII and OVIII (Nicastro et al. 2005). Detection of these so-called “missing baryons” is critical to understanding the matter content of the universe.

Recently it has been suggested that the WHIM gas may be detectable using the Sunyaev-Zeldovich Effect (SZE) (Hernández-Monteagudo et al. 2006; Hallman et al. 2007; Afshordi et al. 2007). The SZE is a consequence of cosmic microwave background (CMB) photons being inverse Compton scattered to higher energy by hot electrons. This upscattering creates a low

frequency decrement in the CMB, and a corresponding higher frequency increment (for review, see e.g., Rephaeli 1995; Birkinshaw 1999; Carlstrom et al. 2002). The SZE is most typically discussed as it relates to observations of clusters of galaxies, since the very hot ($\sim 10^8$ K) gas there is an effective source of high velocity scattering electrons. Detections and analysis of known galaxy clusters have been made by SZE telescopes (e.g., LaRoque et al. 2006; Halverson et al. 2008) and a recent blind search using the South Pole Telescope (SPT) has detected previously unknown galaxy clusters (Staniszewski et al. 2008). Investigators have attempted to estimate the SZE signature of galaxy groups (Moodley et al. 2008) and have made weak detections of supercluster gas in Corona Borealis (Battistelli et al. 2006; Génova-Santos et al. 2005). In addition, much work has been done to study the possibility of using the kinematic SZE to determine both cluster peculiar velocities (Rephaeli & Lahav 1991; Haehnelt & Tegmark 1996; Aghanim et al. 2001) and the overall bulk velocity field (e.g., Kashlinsky & Atrio-Barandela 2000).

Recent work suggests that filaments in large-scale structure, because of their long path lengths and correlated velocities, may have a unique angular power signature in the SZE (Atrio-Barandela et al. 2008). In this paper, we show that the SZE may contribute a detectable signal from the WHIM gas, observable with extensions to the sensitivity of current and upcoming surveys (e.g., SPT, Planck Surveyor) over relatively small angular areas. We examine the contribution of the filamentary WHIM to the angular power spectrum of both the kinematic and the thermal SZE.

¹ National Science Foundation Astronomy and Astrophysics Postdoctoral Fellow

² Center for Astrophysics and Space Astronomy, Department of Astrophysics and Planetary Sciences, University of Colorado at Boulder, Boulder, CO 80309; hallman, burns@casa.colorado.edu

³ Department of Physics and Astronomy, Michigan State University, East Lansing, MI; oshea@msu.edu

⁴ Center for Astrophysics and Space Sciences, University of California at San Diego, La Jolla, CA 92093; mnorman@cosmos.ucsd.edu

1.1. The Relative Strengths of Thermal and Kinematic SZE

The SZE can be separated into two spectrally distinct effects, one which results from the scattering of the CMB by the electrons at the thermal velocity in the gas, and the other resulting from the bulk line-of-sight velocity of the gas (kinematic SZE). Typically for the purposes of clusters of galaxies, the kinematic SZE (kSZE) can be considered a small perturbation on the full SZE signal. However, in the cooler WHIM gas the relative strength of the kSZE increases, becoming comparable to the thermal SZE (tSZE). The reason for this is the different dependency of the kSZE and tSZE on the physical properties of the gas. Indeed, the effects should be comparable when the bulk radial velocity of the gas is roughly equal to the average thermal velocity of the electrons in the gas. The thermal SZE signal, characterized by the Compton y parameter

$$y = \frac{\sigma_T k_B}{m_e c^2} \int n_e T_e dl \quad (1)$$

depends linearly on n_e and T_e (i.e., is proportional to the thermal pressure), while the kinematic SZE, characterized by

$$b = \frac{\sigma_T}{c} \int v_r n_e dl \quad (2)$$

depends linearly on electron density and the line-of-sight peculiar (radial) velocity of the gas. For the kSZE, a negative radial velocity (toward the observer) results in a positive $\Delta T/T$. For the purposes of this work, we study the SZE signals at 150 GHz (2.1 mm), the frequency where the thermal SZE signal has its maximum decrement against the CMB. For the kSZE, the relative temperature shift, $\Delta T/T$, is independent of frequency, and is equal to the value of b . The tSZE value for $\Delta T/T$ is

$$(\Delta T/T)_{tSZE} = y \left(x \frac{e^x + 1}{e^x - 1} - 4 \right), \quad (3)$$

which at 150 GHz is equal to $-y$. Here $x = h\nu/kT$. The thermal SZE is subject to relativistic corrections, which can be important for very hot ($> 10keV$) clusters (Itoh & Nozawa 2004).

If we take the ratio of b/y , the relative strength of the SZE temperature perturbations at 150 GHz, for a given parcel of gas we get

$$\frac{b}{y} = \frac{m_e c v_r}{k_B T_e}. \quad (4)$$

This expression can be written as

$$\frac{b}{y} = 0.197 \frac{v_r/(100km/s)}{T_e/(10^7K)}. \quad (5)$$

A similar calculation is shown in Birkinshaw (1999). For a radial velocity of 100 km/s, and a gas temperature of 5×10^7 K (a temperature typical of clusters), this ratio is around 4 percent. But in a gas having the same radial velocity but a reduced temperature, say a value of $T = 10^6$ K, the ratio is roughly 2. Therefore, for million degree gas with a bulk velocity of 100 km/s along the line of sight, the magnitude of the kSZE component is twice as large as the tSZE. One caveat is that kSZE can

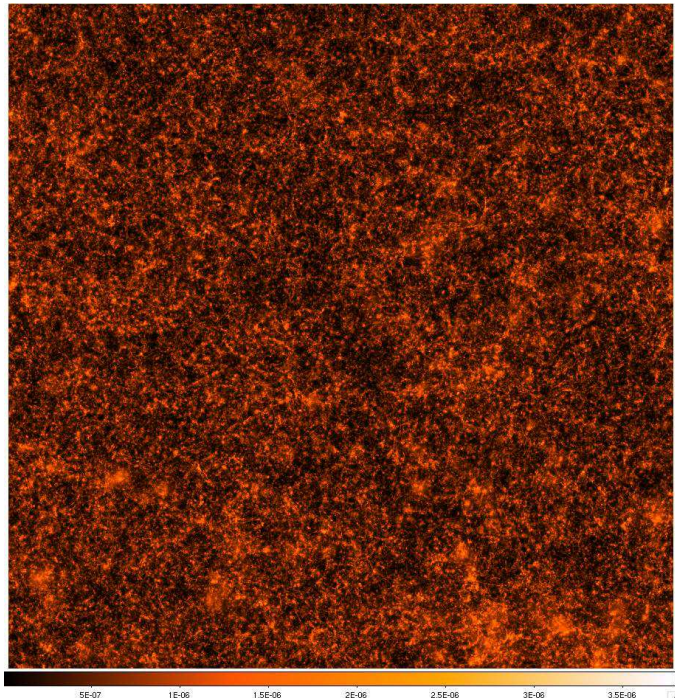


FIG. 1.— Light cone projection for the low-density WHIM (LDW) for the thermal SZE. LDW is defined as $10^5 < T < 10^7$ K and $0 < \delta < 50$. Field spans 10×10 degrees.

be either positive or negative, thus could cancel out the tSZE in some instances. It is possible for the kSZE to be zero when the gas has no peculiar line-of-sight velocity. In addition, gas in cosmological filaments is of relatively low density. However, this gas tends to be more spatially extended, thus there can be very long path lengths, creating a stronger SZE signal. We should note that $\Delta T/T$ for the tSZE is frequency dependent, and on the decrement side at 30 GHz (where interferometers like CARMA operate), $\Delta T/T$ is twice the value of y , while the kSZE has no frequency dependence. Thus at lower frequencies, the ratio of $\Delta T/T$ between kSZE and tSZE is a factor of 2 lower than the b/y indicated above.

It is also perhaps important to note that calculations by Fox & Loeb (1997) and Yoshida et al. (2005) for example, show that in hot gas, the electron temperature may have a non-negligible equilibration time with the (hotter) temperature of the ions in the post-shock regions in filaments. A systematically low electron temperature impacts the thermal SZE signal directly, as it is linear with T_e . The kSZE is unaffected, as it is independent of T_e .

In any case, it is intriguing that the kSZE may serve to boost the tSZE signal of the WHIM gas significantly, perhaps aiding in its detection in a statistical sense through all-sky surveys at the SZE decrement maximum. While it is sometimes advantageous to separate the kSZE and the tSZE by their spectral signatures in order to measure each effect individually, here we also attempt to take advantage of their (sometimes) additive effect in order to aid in the statistical detection of the WHIM gas.

2. SIMULATIONS

The main results shown in this work are from analysis of the Santa Fe Lightcone, described in Hallman et al. (2007). Briefly, this N-body/hydro cosmological simula-

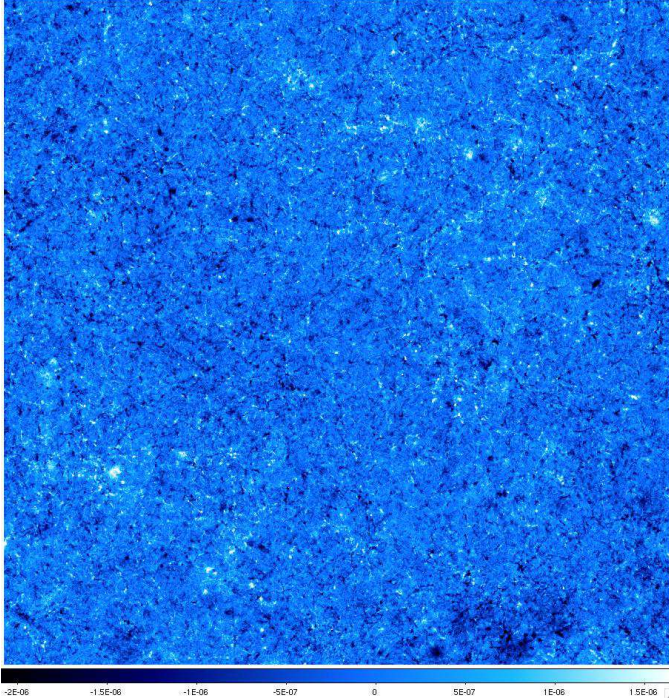


FIG. 2.— Light cone projection for the LDW for the kinematic SZE. Same field as figure 1

tion was carried out with the Enzo (O’Shea et al. 2005) code for the express purpose of generating 100 square (10×10) degree synthetic sky surveys in the SZE and X-rays. The calculation is initialized at $z=99$ using a Eisenstein & Hu (1999) power spectrum with $n = 1$. The cosmological parameters are $\Omega_M = 0.3$, $\Omega_b = 0.04$, $\Omega_{CDM} = 0.26$, $\Omega_\Lambda = 0.7$, $h = 0.7$, and $\sigma_8 = 0.9$. We simulated a cubic volume of dimension $512h^{-1}$ comoving Mpc with a root grid of 512^3 computational zones and seven levels of adaptive refinement using the criteria of baryon and dark matter density. We use 512^3 dark matter particles, resulting in a dark matter mass resolution of $\approx 7.3 \times 10^{10} M_\odot$.

The light cones are made by stacking 27 slices of the simulation data, correcting for their angular scale as a function of their physical size, and taking random projection axis selections and projection translations to get multiple realizations of the light cone for the given cosmology. These slices are projections at various redshifts spanning the range $3.0 > z > 0$. For this work we use 100 realizations of the light cone with random projection axes and shifts. The final light cone images for this work have image resolution of 4096^2 for an effective resolution of $8.8''$ per pixel. From our previous work, we have shown that this simulation effectively resolves the halo mass function down to roughly $5 \times 10^{13} M_\odot$. For more details see Hallman et al. (2007).

2.1. Low-Density WHIM Projections

For this particular work, we have used projections of the thermal and kinematic SZE. We have made light cones from projections of the kSZE and tSZE from gas within the WHIM temperature range ($10^5 - 10^7 K$), and also limit the gas overdensity to the regime from $0 < \delta < 50$ (where δ indicates the overdensity (gas + dark matter) ratio with respect to ρ_c). The limit of 50

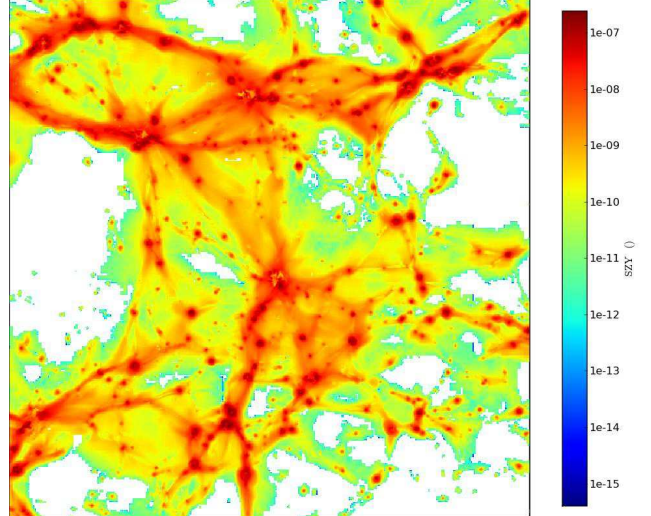


FIG. 3.— Image of the Compton y parameter for the thermal SZE using the low-density WHIM (LDW) gas as described in the text. This projection is made from a slice of the simulation box at $z=0.15$, with a width subtending 10 degrees at that redshift (comoving physical width of $\approx 77h^{-1}$ Mpc), and with a depth of $\approx 128h^{-1}$ Mpc comoving. Illustrates how this range of density and temperature captures the filaments. Projection was made using the YT analysis toolkit (Turk 2008, yt.enzo-tools.org).

serves to remove gas that may be very near clusters. In a Λ CDM cosmology with the currently favored parameter values, this is more than a factor of 3 below the virial overdensity. Therefore the gas we are probing is definitely in the filaments and sheets (and even voids). In our tests of overdensity threshold, we find very weak dependence of the result when changing the overdensity cutoff by a factor of a few. We hereafter refer to this gas as the low-density WHIM (LDW). The LDW light cone projections for the thermal and kinematic SZE are shown in Figures 1 and 2. One reason for the safety factor in selected overdensity is that in any simulation, we have a finite mass resolution, which means that low mass halos are unresolved gravitationally. Therefore the overdensity achieved in the unresolved halos is likely lower than the typical virial value. The main purpose for our choice of limits, therefore, is to ensure that we are fully in the filamentary WHIM regime. Figure 3 shows a projection of a low redshift slice made with the gas properties defined in this way, illustrating how this regime of temperature and density captures the filamentary gas.

3. DETECTING THE SIGNATURE OF THE WHIM WITH PLANCK AND SPT

We first investigate the contribution of the WHIM gas to the SZE signal in a sky survey. The image histograms for the LDW SZE projections are shown in Figure 4. These histograms are from the raw light cone images, which have a native angular resolution of $8.8''$. It is clear that the addition of the kSZE creates a strong increase in the number of pixels above a given flux decrement. The analogous plot for the full SZE projections (for all gas in the simulations) is shown in Figure 5. In this case, the total SZE is dominated by the tSZE, and the kSZE is a small perturbation on that signal. These figures illustrate the argument in Section 1.1 very nicely, i.e. the kSZE is a much more important contributor in the lower density, cooler gas than it is in the hotter cluster gas.

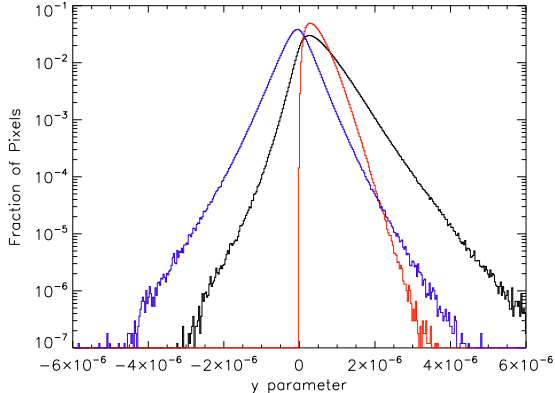


FIG. 4.— Histogram of one of the LDW light cone images in Compton y and/or b parameter. Red line indicates the thermal SZE, blue is for the kinematic SZE, black is the total of the two, an indicator of the total value of $\Delta T/T$ at the thermal decrement maximum ($\approx 2.1\text{mm}/150\text{GHz}$).

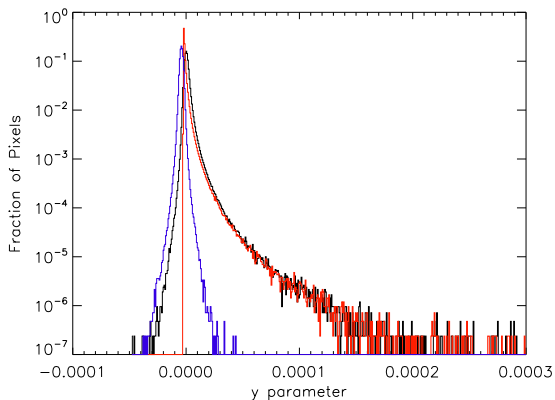


FIG. 5.— Same as Figure 4, but for the full light cone image including clusters. Red is thermal SZE, black total combined signature, and blue is kinematic SZE. Note the relative lack of importance of the kSZE at the high decrement end. This tail is from clusters, where the kSZE is relatively unimportant.

Next, we add the tSZE and kSZE maps, and smooth the light cone maps with a Gaussian kernel where the full width half maximum is equal to the beam size at the thermal SZE decrement maximum for both Planck Surveyor and the South Pole Telescope. We can add the two effects for these purposes (adding y and b) since the relative $\Delta T/T$ at the tSZE maximum decrement is equal to the value of $-y$, and the relative temperature shift due to the kSZE is independent of frequency. Under the assumption that our observation would be made at 150 GHz, this argument is valid.

Finally, we add a white noise component with the rms equal to the expected sensitivity of the two surveys, make a histogram of image values, and attempt to fit a Gaussian to the histogram. If the signal is below the sensitivity of the survey, the fit to a Gaussian should be excellent. If the fit is poor, then a signal has been detected. Figure 6 shows the mean χ^2 values for the Gaussian fitting for 100 realizations of the LDW-only light cone. It is clear that for a four-fold increase in sensitivity in SPT's survey, the LDW makes a real contribution to the sky signal, and at even a factor of 2 increase (to $5\mu\text{K}$ rms

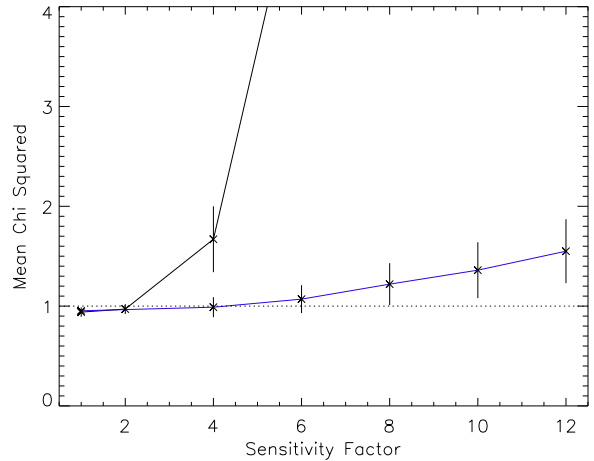


FIG. 6.— The mean value of χ^2 from a Gaussian fit to the image histograms for 100 light cone realizations with error bars indicating the range for 90% of the realizations plotted against the factor by which sensitivity has been increased (i.e. noise rms reduced) over the expected value for each survey. A χ^2 value greater than 1 is indicative of a poor fit to a Gaussian, and that the filaments contribute signal to the maps. Blue is for Planck, black for SPT.

per beam), there might be a marginal detection. Figure 7 shows the result of increasing sensitivity (reducing noise) in the full (10×10 degree) images using the SPT beam size. A sample image histogram for SPT is shown in Figure 8.

For Planck, non-Gaussianity appears marginally at a factor of 8 increase in sensitivity ($0.75 \mu\text{K}$ per beam), and is clearly there at a factor of 10 increase. The difference between these two surveys which favors SPT is the angular scale of the beam. SPT has about an arcminute beam at this frequency, while Planck's is $7.1'$. The scale of the filaments (of order Mpc), which is similar to the cluster scale, is a better match to the SPT beam size for most redshifts. A sample image histogram from an image smoothed to Planck resolution with its Gaussian fit overlaid is shown in Figure 9.

We again note that our simulations assume temperature equilibrium between the ions and electrons, which is probably not achieved on short timescales in this gas. This result should reduce the thermal SZE signature by some amount which is uncertain. A survey would have to be at least as sensitive as what we have described in order to have WHIM contribution to the tSZE signal.

3.1. Methods for Detecting WHIM Gas in SZE Sky Surveys

While it appears clear that at a given survey sensitivity the WHIM gas in filaments (LDW) contributes signal above the noise, it is not initially obvious how such a measurement would be made. In the real universe, we do not have maps of the filaments only, and the lack of redshift diminution in the SZE results in a significant amount of confusion in the survey fields. Therefore, separating the contribution of WHIM from that of clusters and groups of galaxies may seem an insurmountable challenge.

However, it is possible that filaments have a unique angular power signature, such that their contribution could be identified separate from clusters. There are significant difficulties with this approach, as illustrated in Figures

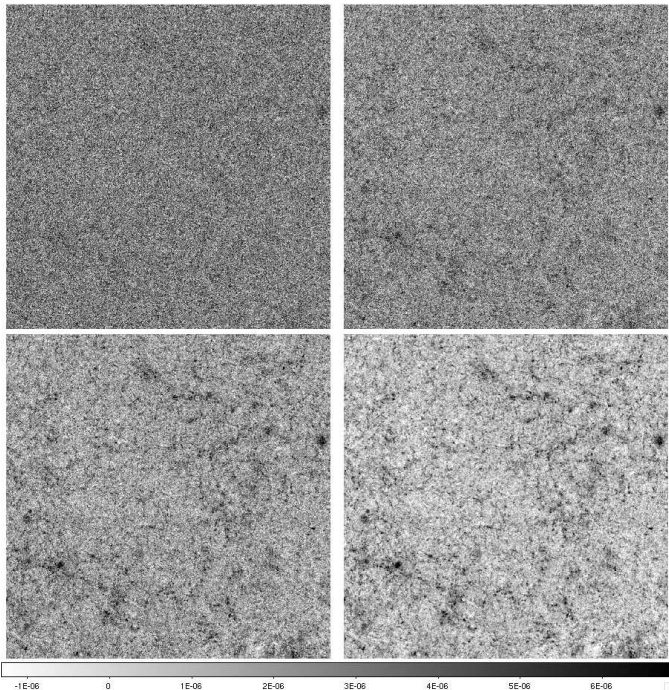


FIG. 7.— Four images of the full 10×10 degree field of the LDW-only light cones in total $\Delta T/T$ smoothed with a $1'$ Gaussian to simulate SPT's beam. Upper left: Image with $10 \mu\text{K}$ rms white noise. Upper right: image with $5 \mu\text{K}$ rms, lower left: image with $2.5 \mu\text{K}$ rms, lower right: $1.25 \mu\text{K}$ rms.

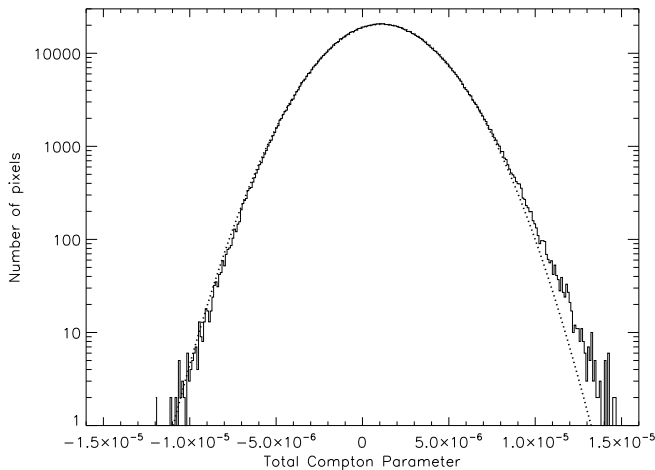


FIG. 8.— Gaussian fit to the image histogram for WHIM light cone with SPT beam and a factor of 4 increase in sensitivity over that expected in SPT's large survey. This is equivalent to a ΔT rms of $2.5 \mu\text{K}$ per beam.

10 and 11. These figures show the relative power for a full simulated sky map and for the low-density WHIM only projections. Figure 10 shows this difference for the tSZE, Figure 11 for the kSZE. While there is a significant amount of gas in the WHIM phase in simulations, they contribute very little to the angular power spectrum, particularly in the tSZE. The angular power at the peak is ~ 3 orders of magnitude lower in the WHIM for the tSZE, and more than a full decade lower for the kSZE. More troublesome is that the shapes of the power spectra are very similar. We should note that for the kSZE, some

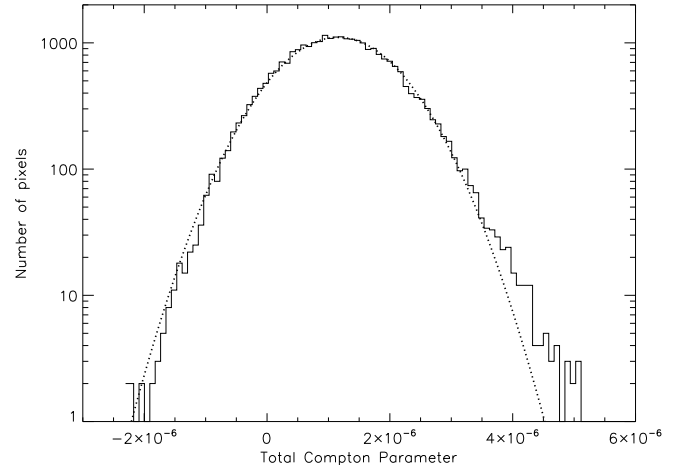


FIG. 9.— Gaussian fit to the image histogram for WHIM light cone with Planck beam and a factor of 8 increase in sensitivity over that expected in Planck's large survey. This is equivalent to a ΔT rms of $0.75 \mu\text{K}$ per beam.

small changes in the stacking algorithm must be made (compared to Hallman et al. (2007)) in order to maintain continuity of structures along the projection depth. This means that no shifting in light cone stacking takes place unless the depth in projection is equal to the depth of the full simulation box.

Indeed, at these large angular scales the SZE is swamped by the primordial CMB anisotropies, and the WHIM contributes a very tiny fraction to the power at these multipoles. What is important to note in these plots is that the prediction of previous investigators of a bump in the angular power spectrum of the kSZE at $l \approx 400$ (Atrio-Barandela et al. 2008) as a result of filaments in the low redshift universe is apparently absent from our result. This is unfortunate, as this bump would create a unique angular signature which one could use to identify the WHIM in filaments. The Atrio-Barandela et al. (2008) work uses an analytic formalism to describe the distribution of gas in filaments, and the distribution of the filaments themselves. It is not clear which assumptions of their model are not reproduced in our simulations, and could account for the discrepancy. We will explore this further in later sections.

It is interesting to note, however, that the relative power in the kSZE and tSZE as a function of gas phase varies dramatically. Figure 12 shows the power spectra for the full light cone maps with tSZE in black and kSZE in blue. Figure 13 shows the same plot for the LDW gas. In this gas, the kSZE dominates at the peak and at most scales. This result meshes nicely with the description of the kSZE/tSZE ratio in Section 1.1.

3.2. Effect of the Low-Density WHIM on the Power Spectrum

Aside from the obvious question of whether the filamentary LDW can be directly detected in SZE surveys, there is the related key issue of the WHIM filaments creating a contaminating signal that might be misinterpreted. For instance, shifts in the SZE angular power spectrum might result in shifts in fitted cosmological parameters (e.g., the value of σ_8). Therefore, it is important to understand the WHIM contribution to the power

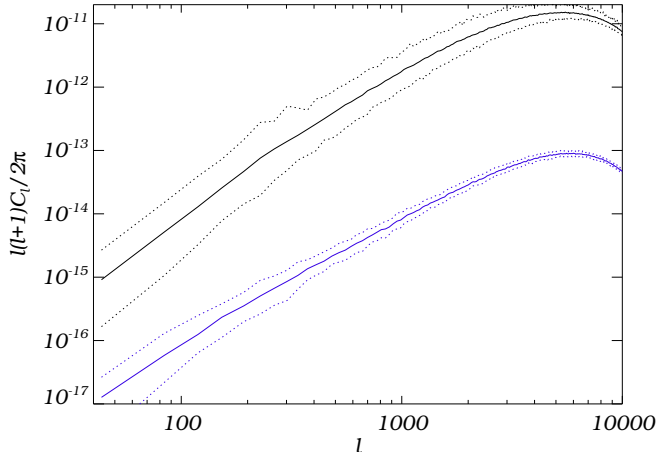


FIG. 10.— Angular power spectra of the thermal SZE from 100 light cone realizations with ranges (dotted) within which 90% of our realizations fall. Black is for projections of the full simulation, blue is for the low-density WHIM as described in the text.

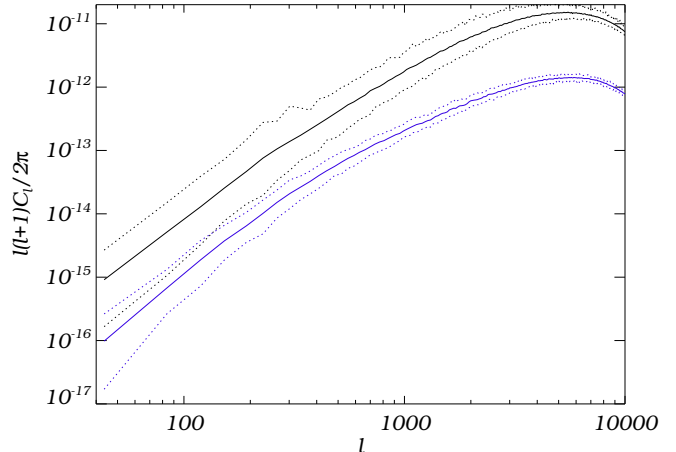


FIG. 12.— Angular power spectra of the full light cone image using all gas in the simulation volume. Black is for the tSZE, blue for the kSZE, with 90% variance of 100 light cone realizations indicated by dotted lines.

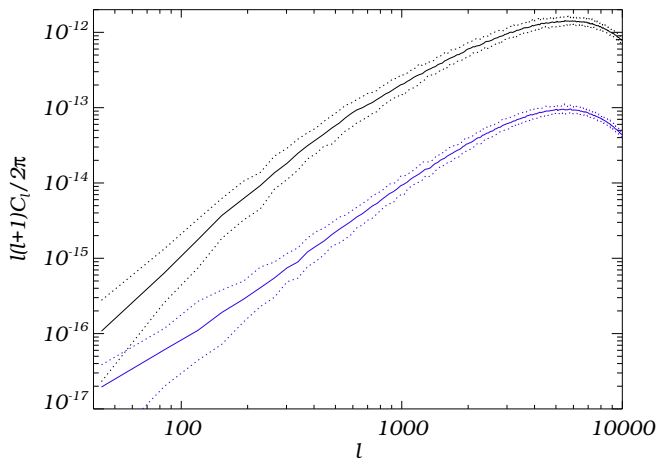


FIG. 11.— Same as Figure 10, but for the kinematic SZE. Blue is the angular power spectrum of the low-density WHIM, black is full light cone, dotted are for the 90% range of 100 light cone realizations.

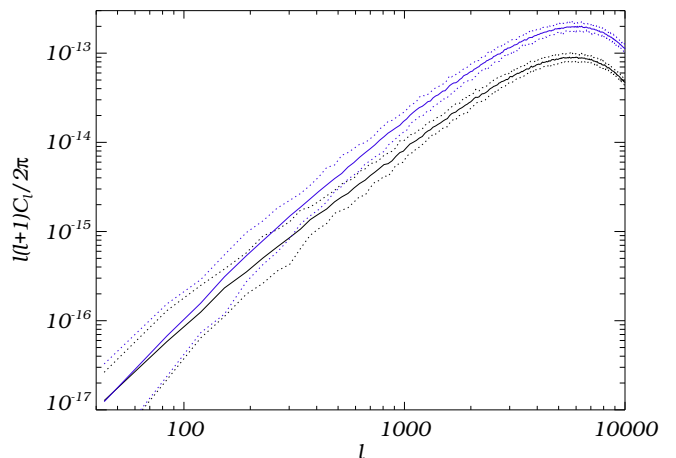


FIG. 13.— Same comparison as Figure 12, but for LDW only light cones. Note that the kSZE has more angular power than the tSZE for the gas in the LDW phase.

spectra.

To investigate this question, we have taken a ratio of our full simulation light cone projection power spectra to power spectra of images where the projection of the LDW SZE has been removed. In all cases we have smoothed the image with a $1'$ Gaussian to represent the beam of SPT at 150 GHz. We have again done this for 100 light cone realizations, and plotted the 90% cosmic variance scatter in the following figures. Figure 14 shows this ratio as a function of multipole number for the thermal SZE. While there is significant cosmic variance at large scales, the mean value (solid line) is a change of order 3% maximum. At high l , the ratio is of order 1%. For the kSZE, the effect is more important. The lines on Figure 15 show the mean and 90% scatter of the power spectra ratios. The removal of the WHIM lowers the overall power in the map by as much as $\approx 8\%$ at $l \approx 100 - 400$. Though declining in contribution to higher l , at $l = 1000$ the effect is still roughly 5%.

3.3. WHIM Power in the kSZE

While this effect is not obvious when looking at the WHIM and total power spectra of the images separately, the range of l where the LDW contributes to the power spectrum is broadly consistent with the results of Atrio-Barandela et al. (2008). Though the cosmic variance using different light cones is quite large, with a large sky area one should see the effect. In Atrio-Barandela et al. (2008), they find a filamentary contribution which moves to lower l as z decreases, as is expected due to the reduced angular diameter distance. Our lowest z defined in these light cones is 0.05, where the filamentary contribution in Atrio-Barandela et al. (2008) appears to peak between $1500 < l < 2000$. We see the change at lower l , where they see the contribution coming from $z < 0.05$. We address this issue further below.

We predict a filamentary WHIM angular power signature consistent with Atrio-Barandela et al. (2008).

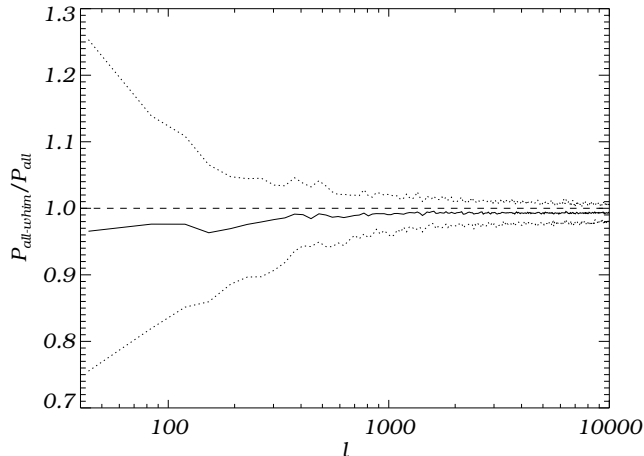


FIG. 14.— Ratio of power spectra from the light cones made from the full simulation box with LDW gas subtracted to those made without subtracting the LDW for the thermal SZE. Dotted lines indicate the 90% cosmic variance in our 100 light cone realizations. While there is large variation at low l , a result of the small volume probed at low z , the mean is consistent with very little change due to the presence of LDW gas.

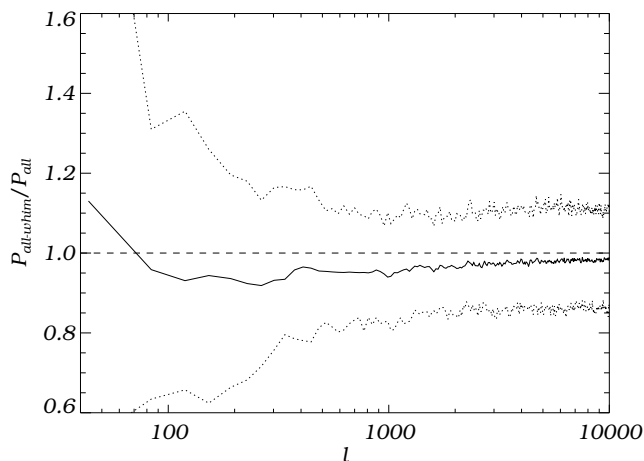


FIG. 15.— Ratio of power spectra as in Figure 14. The removal of the LDW results in a reduction of the power at low multipoles. The effect has a maximum of $\approx 8\%$ at $l \approx 100 - 400$.

There are some differences in the two types of analyses which may be important. First, Atrio-Barandela et al. (2008) integrate the SZE signature of their filamentary models up to relatively high overdensity (300-500), which in our simulation is outside the filamentary regime. In addition, our light cones calculate the SZE signature using a stack of simulation boxes in which the smallest redshift we use is $z=0.05$. That limit means that low redshift filaments, which are largest on the sky, are not represented fully by our method. In their model, the contribution of filaments is a strong function of redshift, low z being most important. Also, in contrast to Atrio-Barandela et al. (2008) we represent a 10×10 degree patch of sky, while their prediction is for an all sky signature.

To explore the potential contribution of foreground filaments, we have added to our light cones a set of 5 images

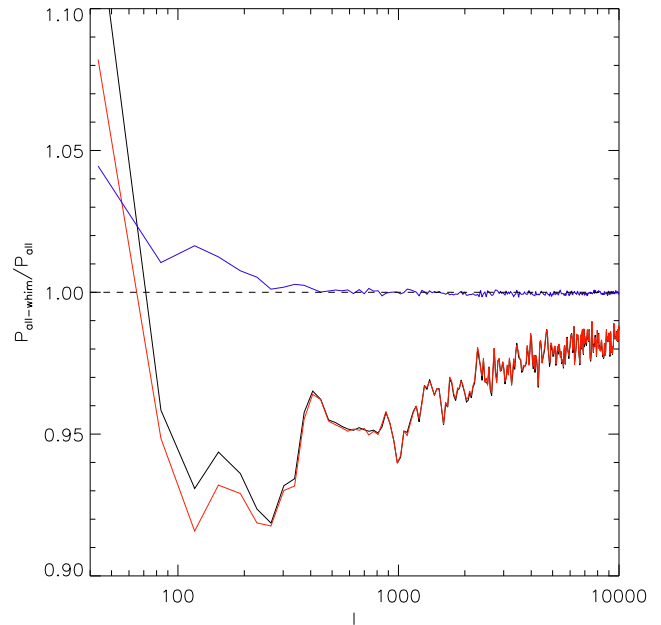


FIG. 16.— Ratio of power spectra as in Figure 15 in black, overlaid with same ratio for light cones adding low z slices as described in the text (red line). 5 kSZ slices are added from $z=0.05$ to $z=0.0$ with a spacing of $\delta z = 0.01$ to investigate the power contribution of near field filaments to the kSZE power spectrum. The blue line is the ratio of the two lines, with the dotted line at equality for illustration. The low redshift filaments do not substantively alter the result.

spanning the redshifts from 0.05 to 0.00 with a δz of 0.01 (simulating the work of Atrio-Barandela et al. (2008)). For this we have used a smaller simulation of a cubic volume of dimension $128h^{-1}\text{Mpc}$ with 256^3 root grid zones and 5 levels of dynamic refinement with refinement criteria similar to those used in the original simulation. This additional simulation is necessary since we have much finer δz spacing, and can then simulate the contribution of low redshift filaments to the kSZ images. For these low redshift slices this volume is more than sufficient, since very little volume is actually sampled in a fixed angular area of 100 square degrees at $z < 0.05$. We have generated 5 fully independent realizations of the slices at the lowest z range described above, and added them to images analyzed in earlier sections. We then repeat the analysis of taking a ratio of power spectra with and without the LDW filaments. The result is shown in Figure 16, and it shows that the addition of low z filaments does not substantively change the results. They simply do not contribute significant power to the overall sky signature in the kSZE.

4. DISCUSSION

While it appears clear that the LDW gas in filaments contributes a real signal to the thermal and kinematic SZE above a certain survey sensitivity, it is unclear how one can take advantage of this effect to “detect” the WHIM gas. The signal associated with the WHIM in the SZE is washed out by the dominant contributions of the hotter, denser gas in clusters and groups, and lies in a wavenumber regime dominated by primary CMB anisotropies. The unique angular signature that the filaments contribute may make their detection in the power

spectrum possible. The WHIM filaments also make a contribution to the kSZE power spectrum that could result in contamination to studies that look to constrain cosmology by the kSZE.

Additionally, it is possible that higher order moments, such as the angular bispectrum or trispectrum (spherical transform of the three- and four-point correlation functions)(e.g., Kogo & Komatsu 2006) of the images, may be more promising measurements of filamentary SZE signatures. If the combined SZE signal of filaments is non-Gaussian (e.g., Yoshida et al. 2001), a three or four-point correlation may show a unique signature of filaments. We leave this analysis to later work.

This simulation has only adiabatic physics and shocks; no non-gravitational physics has been included. However, in this density and temperature regime, cooling times are typically quite long compared to the Hubble time. Also, what are usually considered to be the primary non-gravitational heating mechanisms (stars, AGN) in the universe are found preferentially in high density regions. Therefore, the adiabatic approximation is accurate for this particular problem. However, if episodes of galaxy outflow heating have taken place in this low density gas (as may be indicated by its non-negligible metallicity), then corrections may have to be made. Additionally, the spatial resolution in the low density gas in this particular simulation is not very high. Our root grid simulation zones have spatial extent of 1 Mpc, and gas at between overdensity of 1 and 50 has spatial resolution of between 250 and 500 kpc per zone. Also important is our mass resolution, which means that low mass (under $5 \times 10^{13} M_{\odot}$) clusters are gravitationally under-resolved. Therefore, gas which is in filaments in our simulation may properly belong in collapsed structures like galaxies. It is not immediately clear which direction these effects would push the results, since higher spatial resolution of the filaments would result in higher density, increasing the WHIM SZE signal, and higher mass resolution should result in less gas in the WHIM phase overall. We will study these questions in later papers.

5. SUMMARY

Low-density WHIM gas in filaments contributes signal to 100+ square degree sky surveys if the sensitivity is sufficiently high. This contribution becomes important for an SPT-like telescope survey when the sensitivity is increased by as little as a factor of 2-4x. In the filaments,

the kinematic SZE becomes quite important relative to the thermal SZE, particularly in the frequency regime of maximum thermal SZE decrement (150 GHz) where SZE surveys are being performed. In some phases of the gas, the kSZE can be the dominant contributor to the SZE signal at that wavelength.

The presence of WHIM gas in filaments modifies the kinematic SZE angular power spectrum by $\approx 8\%$ at $l > 100 - 400$. Our results are broadly consistent with the prediction of Atrio-Barandela et al. (2008) of the $l \approx 400$ bump in the kSZE angular power spectrum due to filaments. The thermal SZE is less affected by the presence of filaments. The modification of the kSZE angular power spectrum could be a source of error in cosmological parameters derived from the kSZE. It is likely that this bias can be corrected using numerical simulations like those described in this work. The unique angular signature of the WHIM filaments in the kSZE may allow for WHIM detection using kSZE surveys provided systematic effects can be accounted for with high accuracy, and a clever method of isolating the effect from that due to clusters can be devised.

BWO and MLN have been supported in part by NASA grant NAG5-12140 and NSF grant AST-0307690. BWO has been funded in part under the auspices of the U.S. Dept. of Energy, and supported by its contract W-7405-ENG-36 to Los Alamos National Laboratory. BWO is supported in part by the NASA ATFP program under grant NNX09AD80G. The simulations were performed by SDSC and NCSA with computing time provided by NRAC allocation MCA98N020. This work was partially supported by the National Institute for Computational Sciences (NICS) under TG-AST090040 and utilized the NICS Kraken system. EJH and JOB have been supported in part by a grant from the U.S. National Science Foundation (AST-0407368). JOB acknowledges support from NSF AST-0807215. EJH also acknowledges support from NSF AAFP AST-0702923. BDS was supported by NASA Theory grant NNX07AG77G. Projections were made using the YT analysis toolkit (Turk 2008, yt.enzotools.org). EJH acknowledges useful discussions with Nils Halverson, Sam Skillman, Licia Verde and Liliya Williams. We also acknowledge the insightful comments of an anonymous referee in improving the manuscript.

REFERENCES

- Afshordi, N., Lin, Y.-T., Nagai, D., & Sanderson, A. J. R. 2007, *MNRAS*, 378, 293
- Aghanim, N., Górski, K. M., & Puget, J.-L. 2001, *A&A*, 374, 1
- Atrio-Barandela, F., Mücke, J. P., & Génova-Santos, R. 2008, *ApJ*, 674, L61
- Battistelli, E. S., De Petris, M., Lamagna, L., Watson, R. A., Rebolo, R., Melchiorri, F., Génova-Santos, R., Luzzi, G., De Gregori, S., Rubiño-Martín, J. A., Davies, R. D., Davis, R. J., Grainge, K., Hobson, M. P., Saunders, R. D. E., & Scott, P. F. 2006, *ApJ*, 645, 826
- Turk, M. 2008, in *Proceedings of the 7th Python in Science Conference*, ed. G. Varoquaux, T. Vaught, & J. Millman, (Pasadena, CA: SciPy), 46, <http://conference.scipy.org/proceedings/SciPy2008/paper-11/>
- Birkinshaw, M. 1999, *Phys. Rep.*, 310, 97
- Carlstrom, J. E., Holder, G. P., & Reese, E. D. 2002, *ARA&A*, 40, 643
- Cen, R. & Ostriker, J. P. 1999, *ApJ*, 514, 1
- Danforth, C. W. & Shull, J. M. 2005, *ApJ*, 624, 555
- , 2008, *ApJ*, 679, 194
- Davé, R., Cen, R., Ostriker, J. P., Bryan, G. L., Hernquist, L., Katz, N., Weinberg, D. H., Norman, M. L., & O’Shea, B. 2001, *ApJ*, 552, 473
- Eisenstein, D. J. & Hu, W. 1999, *ApJ*, 511, 5
- Fox, D. C. & Loeb, A. 1997, *ApJ*, 491, 459
- Génova-Santos, R., Rubiño-Martín, J. A., Rebolo, R., Cleary, K., Davies, R. D., Davis, R. J., Dickinson, C., Falcón, N., Grainge, K., Gutiérrez, C. M., Hobson, M. P., Jones, M. E., Kneissl, R., Lancaster, K., Padilla-Torres, C. P., Saunders, R. D. E., Scott, P. F., Taylor, A. C., & Watson, R. A. 2005, *MNRAS*, 363, 79
- Haehnelt, M. G. & Tegmark, M. 1996, *MNRAS*, 279, 545

- Hallman, E. J., O'Shea, B. W., Burns, J. O., Norman, M. L., Harkness, R., & Wagner, R. 2007, *ApJ*, 671, 27
- Halverson, N. W., Lanting, T., Ade, P. A. R., Basu, K., Bender, A. N., Benson, B. A., Bertoldi, F., Cho, H. ., Chon, G., Clarke, J., Dobbs, M., Ferrusca, D., Guesten, R., Holzappel, W. L., Kovacs, A., Kennedy, J., Kermish, Z., Kneissl, R., Lee, A. T., Lueker, M., Mehl, J., Menten, K. M., Muders, D., Nord, M., Pacaud, F., Plagge, T., Reichardt, C., Richards, P. L., Schaaf, R., Schilke, P., Schuller, F., Schwan, D., Spieler, H., Tucker, C., Weiss, A., & Zahn, O. 2008, *ArXiv e-prints*
- Hernández-Monteagudo, C., Trac, H., Verde, L., & Jimenez, R. 2006, *ApJ*, 652, L1
- Itoh, N. & Nozawa, S. 2004, *A&A*, 417, 827
- Kashlinsky, A. & Atrio-Barandela, F. 2000, *ApJ*, 536, L67
- Kogo, N. & Komatsu, E. 2006, *Phys. Rev. D*, 73, 083007
- LaRoque, S. J., Bonamente, M., Carlstrom, J. E., Joy, M. K., Nagai, D., Reese, E. D., & Dawson, K. S. 2006, *ApJ*, 652, 917
- Moodley, K., Warne, R., Goheer, N., & Trac, H. 2008, *ArXiv e-prints*
- Nicastro, F., Mathur, S., Elvis, M., Drake, J., Fiore, F., Fang, T., Fruscione, A., Krongold, Y., Marshall, H., & Williams, R. 2005, *ApJ*, 629, 700
- O'Shea, B. W., Bryan, G., Bordner, J., Norman, M. L., Abel, T., Harkness, R., & Kritsuk, A. 2005, in *Adaptive Mesh Refinement: Theory and Applications* (Berlin: Springer), 341
- Rephaeli, Y. 1995, *ARA&A*, 33, 541
- Rephaeli, Y. & Lahav, O. 1991, *ApJ*, 372, 21
- Staniszewski, Z., Ade, P. A. R., Aird, K. A., Benson, B. A., Bleem, L. E., Carlstrom, J. E., Chang, C. L., Cho, H. ., Crawford, T. M., Crites, A. T., de Haan, T., Dobbs, M. A., Halverson, N. W., Holder, G. P., Holzappel, W. L., Hrubes, J. D., Joy, M., Keisler, R., Lanting, T. M., Lee, A. T., Leitch, E. M., Loehr, A., Lueker, M., McMahon, J. J., Mehl, J., Meyer, S. S., Mohr, J. J., Montroy, T. E., Ngeow, C. ., Padin, S., Plagge, T., Pryke, C., Reichardt, C. L., Ruhl, J. E., Schaffer, K. K., Shaw, L., Shirokoff, E., Spieler, H. G., Stalder, B., Stark, A. A., Vanderlinde, K., Vieira, J. D., Zahn, O., & Zenteno, A. 2008, *ArXiv e-prints*
- Tripp, T. M., Sembach, K. R., Bowen, D. V., Savage, B. D., Jenkins, E. B., Lehner, N., & Richter, P. 2008, *ApJS*, 177, 39
- Yoshida, N., Furlanetto, S. R., & Hernquist, L. 2005, *ApJ*, 618, L91
- Yoshida, N., Sheth, R. K., & Diaferio, A. 2001, *MNRAS*, 328, 669